ELSEVIER

Journal of Structural Geology 29 (2007) 288–297

JOURNAL OF STRUCTURAL GEOLOGY

www.elsevier.com/locate/jsg

Effects of overburden on joint spacing in layered rocks

A. Jain, B.B. Guzina, V.R. Voller*

Department of Civil Engineering, University of Minnesota, 500 Pillsbury Drive S.E., Minneapolis, MN 55455, USA

Received 24 December 2005; received in revised form 18 August 2006; accepted 28 August 2006
Available online 7 November 2006

Abstract

When a layered system of rock beds is subjected to a sufficiently large extensional strain, joints form in the competent layers. Previous analyses have shown that the ratio between joint spacing and competent layer thickness decreases as the applied strain increases. Further, if the entire interface between the competent layer and the matrix fails in shear (slip), no new joints can form and a lower bound on the joint spacing is reached. In this paper, a joint spacing analysis is developed to explicitly account for the effects of overburden depth. The resulting model is a pair of non-linear equations that can be solved for the characteristic joint spacing as a function of layer thickness, applied strain, and overburden depth. The model results show that, for a given applied strain, the joint spacing first decreases and then increases with depth. This behavior is controlled by the opposing effects of depth-increasing shear strength along the competent layer–matrix interface and depth-increasing compressive prestress. The analysis also reveals that the lower bound (saturation) joint spacing is strongly dependent on depth. Within the choice of realistic physical parameters, predicted values of the saturation-spacing-to-layer-thickness ratio span the range of values observed in the field.

Keywords: Joint spacing; Tectonic strain; Shear-lag; Interfacial slip

1. Introduction

When layered rocks are subjected to an extensional strain in a direction parallel to the layers, tensile stresses are induced (Hobbs, 1967; Mandal et al., 1994; Ji and Saruwatari, 1998; Bai et al., 2000; Bai and Pollard, 2000a,b). Within the framework of elastic system response, the level of tensile stress achieved will naturally depend on the value of the elastic (Young's) modulus. In a layered system consisting of two rock types, the stresses will be larger in the layer with the larger modulus (the competent layer) and lower in adjacent layers with a smaller modulus (incompetent layers). When the tensile stress in the competent layer reaches its tensile strength, joints will form thereby relieving the stress. Observations indicate that the spacing between joints in layered rocks is relatively uniform and exhibits a characteristic length scale associated with the applied strain (Hobbs, 1967; Mandal et al., 1994; Zhao and Ji, 1997; Ji and Saruwatari, 1998).

If the spacing between joints is larger than the thickness of the competent layer, an explanation for this behavior can be obtained using the so-called "shear-lag" model first proposed by Cox (1952) in the study of fibers in paper. A recent example can be found in Ji and Saruwatari (1998), Ji et al. (1998) who extended previous work by Hobbs (1967) to develop a model that, on input of layer geometry and elastic properties, predicts the characteristic spacing between joints. On using values from the measured ranges of modulus and strength of rock layers (see Figs. 7 and 8), an estimation of the tectonic strain imposed on Earth's crust was made by matching results from the analysis to field observations of joint spacing. While Ji and Saruwatari (1998) assumed perfect bonding between the rock layers as in earlier analyses, the model in Ji et al. (1998) is noteworthy since it represents the first attempt at including the effect of slip between the competent and matrix layers. An apparent limitation in this work, however, is that the influence of the depth of the overburden is not explicitly accounted

* Corresponding author. Tel.: +1 612 625 0764.
E-mail address: volle001@umn.edu (V.R. Voller).

0191-8141/$ - see front matter © 2006 Elsevier Ltd. All rights reserved.
doi:10.1016/j.jsg.2006.08.010

for. This depth could influence the predicted joint spacing in two ways. If a Mohr–Coulomb slip failure criterion is used (e.g. Goodman, 1989), the value of the layer–matrix interfacial shear strength will, through the normal stress in the friction term, increase with depth of the overburden. This increase will in turn lead to a higher tensile stress in the competent layer associated with a given extensional strain and thereby decrease the predicted joint spacing. On the other hand, an increasing overburden pressure will also induce a higher (horizontal) compressive prestress in the competent layer as predicted by the Poisson effect in elasticity (e.g. Malvern, 1969) whereby a body subject to uniaxial compression exhibits extensional strain in the transverse direction. The increase of this compressive prestress, which can be assumed to be uniform in the lateral direction, will mean that an observed joint spacing in the competent layer is associated with a larger tectonic strain. Hence, it is expected that the incorporation of Mohr–Coulomb slip and initial prestress in the analysis will result in a dependence of the characteristic joint spacing on the overburden depth of the competent layer; a dependence that is not investigated in earlier studies (Hobbs, 1967; Ji and Saruwatari, 1998; Ji et al., 1998; Bai et al., 2000; Bai and Pollard, 2000a,b).

Recently, a semi-analytical model for the crack spacing in a thermally-shrinking thin film section placed on a thermally inert substrate has been proposed and tested in the materials literature (Timm et al., 2003; Guzina et al., 2004). In this model, the interface between the film and substrate is allowed to slip if the contact shear stress exceeds a threshold value. As examined in Timm et al. (2003), this is achieved by using a generalized Winkler foundation, consisting of a series of sliders and springs, to describe and account for the interface and interaction between the film and its substrate. This model assumes a Mohr–Coulomb failure criterion for the film–substrate interface and incorporates the effect of a pre-existing (e.g. residual) stress through an appropriate reduction of the effective tensile strength of the film. The major objective of this paper is to extend the methodology of Timm et al. (2003) and develop a model for joint spacing in geological systems that explicitly accounts for the depth of overburden through (i) the Mohr–Coulomb failure criterion controlling the slip between the competent and matrix layers, and (ii) the presence of horizontal compressive prestress in the competent layer.

Shear-lag models have been extensively used, verified, and experimentally validated across a range of physical and natural systems (e.g. Hu and Evans, 1989; Chen et al., 1999; Timm et al., 2003; Guzina et al., 2004). When incorporating the effects of layer slip and initial compressive prestress one must keep in mind, however, that the validity of the one-dimensional analyses underlying "conventional" (i.e. no-slip) shear-lag models requires that the spacing between joints be larger than the thickness of the jointed layer. Indeed, as demonstrated by the two-dimensional finite element analysis of bonded layers in Bai et al. (2000), when the spacing-to-thickness ratio falls below unity a compressive stress develops locally between the joints; a state that will prevent the formation of additional joints. In this way, Bai et al. (2000) and Bai and Pollard (2000a,b) suggest that the spacing-to-thickness ratio of approximately 1 corresponds to *joint saturation*, i.e. the situation where a further increase in tectonic strain will not lead to the formation of additional joints. In contrast, a shear-lag model where the interfacial slip is likewise neglected (e.g. Ji and Saruwatari, 1998) will, under an increasing strain, continue to form joints, down to the limit of zero joint spacing, well below the point where one would expect the shear-lag model to be valid. With the incorporation of interfacial slip, however, the shear-lag model does result in a non-zero saturation joint spacing (Ji et al., 1998). In physical terms, when the applied strain goes beyond the point where the entire interface between an intact segment of the competent layer and the matrix fails in slip, there is no additional stress transfer and consequently no new joints can form. This alternative explanation for saturation spacing has been validated (Timm et al., 2003; Guzina et al., 2004) for other physical systems. In this study, the featured (slip-based) saturation mechanism will be shown to be valid for *all* joint spacing-to-thickness ratios in layered rock beds.

In the next section, the groundwork for the model development is provided and a theoretical argument as to why there should be a characteristic joint spacing is presented. This is followed by a full theoretical development of the model by building on the earlier works of Ji and Saruwatari (1998), Ji et al. (1998), Timm et al. (2003) and Guzina et al. (2004). Analysis with the revised model reveals that both the joint spacing and its saturation limit are strongly dependent on the overburden depth. Within the choice of realistic physical parameters, predicted values of the saturation-spacing-to-layer-thickness ratio span the range of values observed in the field.

2. Stress development and cracking of a competent layer

The objectives of this section are to (i) establish a general elastic-slip model for the stress state in a layered rock system subject to extensional strain, and (ii) use the model to describe how joints form and why there is a characteristic spacing between the joints.

To develop the necessary model, consider a layered rock system shown in Fig. 1a consisting of alternating incompetent, i.e. "soft" layers (so-called matrix) and their competent, i.e. "stiff" counterparts. The matrix layers have thickness d, Young's modulus E_m, and Poisson's ratio ν_m; the competent layers are characterized by thickness t, Young's modulus $E_c > E_m$, and Poisson's ratio ν_c. The breadth (the out of plane dimension) of the system is b; its (constant) unit weight is denoted by $\gamma = \rho g$, where ρ is the density of the rock and g stands for gravitational acceleration. In the absence of an applied extensional strain, the layered system is characterized by natural joints in the competent layer, resulting in an initially undamaged section of the competent layer of length λ. For consistency with earlier works, it is assumed $\lambda \gg b$ so that the plane stress approximation can be used in the analysis. With reference to Fig. 1b, the representative (cut-out) domain

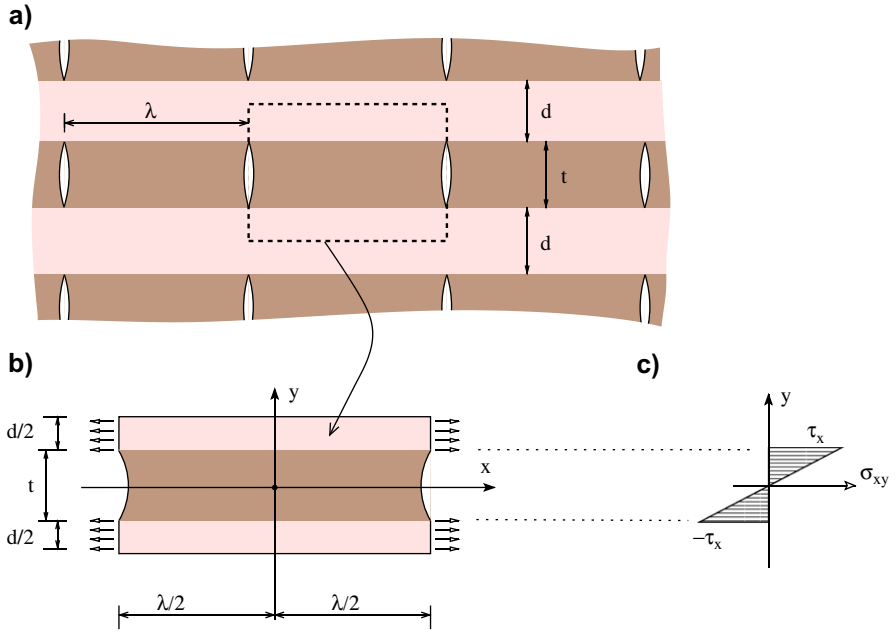

Fig. 1. Schematic of (a) the layered bed system, (b) representative domain, and (c) approximate shear stress distribution at a section $x = \text{const.}$ in the competent layer. Dark gray is the competent layer, and light gray indicates the matrix.

of the system consists of a single competent layer sandwiched between two matrix half-layers of thickness $d/2$. In this system, horizontal axial stress is induced by displacing the end sections of the matrix layers, located at $x = \pm\lambda/2$, by the respective amounts $\pm\Delta_x$ while keeping the end sections of the competent layer traction-free. In this way the matrix layers are subjected to an average extensional strain $\epsilon = 2\Delta_x/\lambda$. Further, through symmetry, any subsequent analysis can be carried out by restricting attention to the rectangular domain

$$0 \le x \le \frac{\lambda}{2}, \quad -\frac{t+d}{2} \le y \le \frac{t+d}{2},$$

subject to the boundary conditions

$$\begin{aligned}
&u_x = 0, \quad \sigma_{xy} = 0, \quad x = 0, && 0 \le |y| \le \frac{t+d}{2},\\
&u_x = \Delta_x, \ u_y = 0, \quad x = \frac{\lambda}{2}, && \frac{t}{2} < |y| \le \frac{t+d}{2},\\
&\sigma_{xx} = 0, \quad \sigma_{xy} = 0, \quad x = \frac{\lambda}{2}, && 0 \le |y| < \frac{t}{2},\\
&\tau_{xy} = 0, \quad \sigma_{yy} = -p, \ 0 \le x \le \frac{\lambda}{2}, && |y| = \frac{t+d}{2},
\end{aligned} \tag{1}$$

where $u_x(x,y)$ and $u_y(x,y)$ are the horizontal and vertical displacements; $p(h)$ denotes the overburden pressure; h is the depth of the overburden at the origin of the local system ($x = y = 0$); $\sigma_{xx}(x,y)$ and $\sigma_{yy}(x,y)$ are the tensile stresses in the x and y directions, and $\sigma_{xy}(x,y)$ is the associated shear stress.

For the ensuing analysis, it is useful to introduce the auxiliary variables

$$\begin{aligned}
&\sigma_x \equiv \sigma_x(x) = \frac{1}{t}\int_{-t/2}^{t/2} \sigma_{xx}(x,y)\,\mathrm{d}y,\\
&\overline{u}_x \equiv \overline{u}_x(x) = \frac{1}{t}\int_{-t/2}^{t/2} u_x(x,y)\,\mathrm{d}y, \qquad -\frac{\lambda}{2} < x < \frac{\lambda}{2}\\
&\tau_x \equiv \tau_x(x) = \sigma_{xy}\left(x, \frac{t}{2}\right)
\end{aligned} \tag{2}$$

where σ_x and $\overline{u}_x$ denote, respectively, the *average* normal stress and axial displacement in the competent layer at a cross-section $x = \text{const.}$ Owing to the problem symmetry with respect to the y-axis which requires that $\sigma_{xy}(x,-y) = -\sigma_{xy}(x,y)$ (see e.g. Malvern, 1969), one further finds that the average of the shear stress and its derivative with respect to x in the competent layer both vanish, i.e.

$$\frac{\mathrm{d}}{\mathrm{d}x}\left\{\frac{1}{t}\int_{-t/2}^{t/2} \sigma_{xy}(x,y)\,\mathrm{d}y = 0\right\} \Rightarrow \frac{1}{t}\int_{-t/2}^{t/2} \frac{\partial \sigma_{xy}(x,y)}{\partial x}\,\mathrm{d}y = 0. \tag{3}$$

To approximate the two-dimensional (2D) problem in Fig. 1b in terms of a simplified 1D model, a key assumption is next made that the variation of the shear stress, σ_{xy}, in the competent layer is *approximately linear* with y (see, e.g. Bai and Pollard, 2000a) so that

$$\frac{\partial \sigma_{xy}(x,y)}{\partial y} \approx \frac{2\tau_x}{t} \Rightarrow \frac{1}{t}\int_{-t/2}^{t/2} \frac{\partial \sigma_{xy}(x,y)}{\partial y}\,\mathrm{d}y \approx \frac{2\tau_x}{t}, \tag{4}$$

as illustrated in Fig. 1c. On the basis of Eqs. (2)–(4), the 2D equilibrium equations for the competent layer with zero body

force, when integrated with respect to y, degenerate to an *uncoupled* format

$$\begin{aligned}\frac{\partial\sigma_{xx}}{\partial x}+\frac{\partial\sigma_{xy}}{\partial y}=0\\ \frac{\partial\sigma_{xy}}{\partial x}+\frac{\partial\sigma_{yy}}{\partial y}=0\end{aligned}\Rightarrow\frac{1}{t}\int_{-t/2}^{t/2}(\cdot)\mathrm{d}y\Rightarrow\begin{aligned}\frac{\mathrm{d}\sigma_x}{\mathrm{d}x}+\frac{2\tau_x}{t}=0,\\ \int_{-t/2}^{t/2}\frac{\partial\sigma_{yy}(x,y)}{\partial y}\mathrm{d}y=0\end{aligned}, \quad (5)$$

With reference to the boundary conditions in Eq. (1), the second equation of the new (integrated) system is identically satisfied by taking $\sigma_{yy}(x,y)=-p=\text{const}$. Accordingly, the equilibrium problem at hand is effectively reduced to an ordinary differential equation

$$\frac{\mathrm{d}\sigma_x}{\mathrm{d}x}=-\frac{2\tau_x}{t},\quad 0\le x\le\frac{\lambda}{2}; \quad (6)$$

in terms of the *average* axial stress, σ_x, subject to the boundary condition

$$\sigma_x\left(\frac{\lambda}{2}\right)=0. \quad (7)$$

Through the above derivation it is shown that the ensuing 1D shear-lag model, satisfying Eqs. (6) and (7), is mechanically valid as it conforms with the 2D static equilibrium in an average (i.e. integral) sense *regardless* of the functional variation underlying $\tau_x(x)$. It is further noted that the average normal stress, σ_x, and the average shear stress, $1/t\int_{-t/2}^{t/2}\sigma_{xy}(x,y)\mathrm{d}y$, are both zero at the fracture face ($x=\lambda/2$) since the latter quantity vanishes identically by virtue of Eq. (3). In this way the perceived inconsistencies of the shear-lag model, examined in Bai and Pollard (2000a), are circumvented by interpreting the featured variables in an *average* rather than a local sense.

At this point the outcome of the 1D model, i.e. the solution of Eqs. (6) and (7), is controlled by the specification of the interfacial shear stress τ_x. In general, $\tau_x(x)$ will depend on (i) material properties of the matrix and competent layer; (ii) geometry of the system; (iii) average extensional strain, ϵ, of the matrix, and (iv) mechanical response of the layer interface to loading. In all cases, however, it is expected that the interfacial shear stress τ_x will take the value of zero at $x=0$ and increase to a maximum value at $x=\lambda/2$. For example, using the model described in Section 3 with $\lambda/t=10$, if an elastic response and a perfect bonding between the matrix and competent layer are assumed, the shear stress will increase monotonically as shown in curve "a" of Fig. 2.

A more realistic assumption for the interface response is to allow for the slip to occur between the matrix and competent layer at sections where the shear stress τ_x reaches a given threshold τ_f. In this case, as shown in curves "b" and "c" of Fig. 2, beyond the point $x=x_t$, where the threshold value is reached, the interface shear stress takes a constant value τ_f. For completeness, it can be shown by virtue of the equilibrium Eq. (6) that all cases in Fig. 2 result in a monotonic decrease in the average axial stress, from a value of $\sigma_x=\sigma_{x,\max}$ at $x=0$ to a value of $\sigma_x=0$ at $x=\lambda/2$, see Fig. 3.

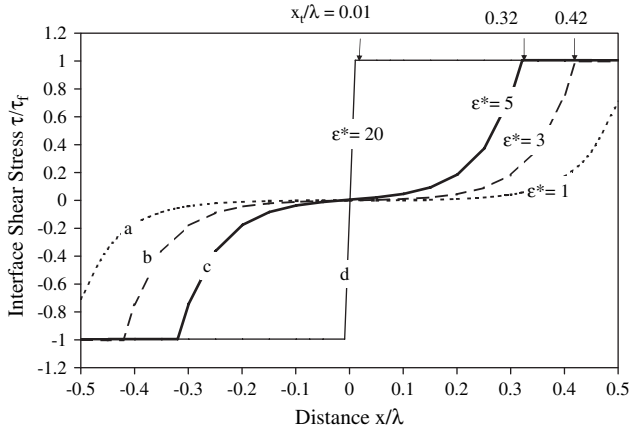

Fig. 2. Shear stress along the layer–matrix interface with increasing applied strain $\epsilon^*=(E_c/\tau_f)\epsilon$; $x=x_t$ on curves b, c and d indicates the onset of slip.

As the extension in the matrix (i.e. average strain ϵ) is increased, the maximum value of $\sigma_x(x)$ at the center of the competent layer will increase; at some point in the process, the maximum stress will reach the tensile strength S of the competent layer, and the latter will split into two parts. For a given material and geometric configuration (i.e. layer elastic moduli and thicknesses), the maximum stress that can be reached in the competent layer will increase with intact length of the competent layer. In this way, for a given strain ϵ, there is a characteristic segment length, $\lambda_c(\epsilon)$, for which the maximum stress in the middle of the segment is

$$\sigma_{x,\max}=S.$$

As a result, competent layer segments longer than $\lambda_c(\epsilon)$ will necessarily break in two. In contrast, the maximum stress in competent segments shorter than $\lambda_c(\epsilon)$ will not reach the limiting value of S, and such segments will remain intact. Accordingly, a competent layer with an initial segment length $\lambda>\lambda_c(\epsilon)$ will, when its associated matrix is subjected to an average extensional strain ϵ, form joints with a spacing bounded by

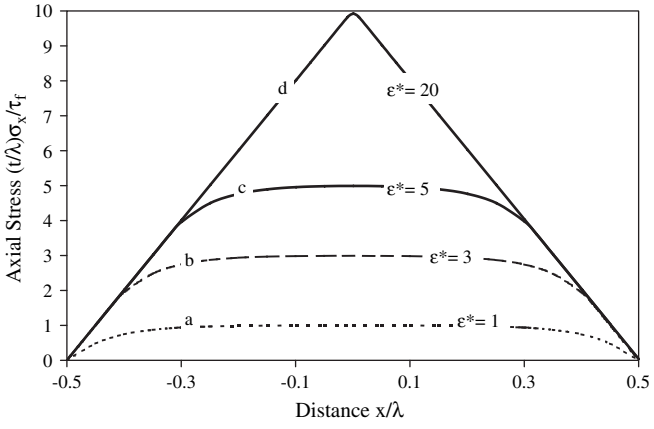

Fig. 3. Axial stress distribution in the competent layer with increasing applied strain $\epsilon^*=(E_c/\tau_f)\epsilon$.

$$\frac{\lambda_c(\epsilon)}{2} \le \lambda \le \lambda_c(\epsilon), \tag{8}$$

so that the *average* joint spacing is

$$\overline{\lambda}_c = 0.75\lambda_c(\epsilon). \tag{9}$$

3. Stress model for the competent layer including overburden

If the effects of overburden are taken into account, the initial *horizontal* compressive stress induced in the competent layer at depth h can be calculated, using the premise of plane stress, as $\nu_c\gamma h$ where γ is the (average) unit weight of the layered system and ν_c is the Poisson's ratio of the competent layer (e.g. Malvern, 1969). In this way the maximum intact segment length $\lambda_c(\epsilon, h)$ corresponds to the segment in which the maximum stress is

$$\sigma_{x,\max} = S' \equiv S + \nu_c\gamma h. \tag{10}$$

Beyond Eq. (10), the key to obtaining a model that can predict the characteristic joint spacing λ_c in Eq. (8) involves a specification of the interfacial shear stress τ_x in Eq. (6), and a solution for the axial stress σ_x in the competent layer that satisfies Eqs. (6) and (7). A modeling tool that allows for the specification of an interfacial shear stress which can account for a slip between the competent layer and the matrix is to divide the featured interface segment $0 \le x \le \lambda/2$ into two distinct sections, namely a non-slip (elastic reaction) zone, $0 \le x \le x_t$, and a sliding region, $x_t \le x \le \lambda/2$.

These regions can be modeled using a mechanical analog, namely a generalized Winkler foundation (Timm et al., 2003), where the interface is replaced by a sequence of sliders in the slip region and a sequence of springs in the non-slip region, see Fig. 4. In this way, Eq. (6) can be written as

$$\frac{d\sigma_x}{dx} = -\begin{cases} \dfrac{2k(v_x - \overline{u}_x)}{A}, & 0 \le x \le x_t \\ \dfrac{2\tau_f}{t}, & x_t \le x \le \dfrac{\lambda}{2} \end{cases}, \tag{11}$$

where $A = tb$ is the cross-sectional area of the competent layer. The numerator of the first component on the right-hand-side of Eq. (11) can be viewed as a the product of a "spring" constant k and a relative displacement, $(v_x - \overline{u}_x)$, between the matrix and the competent layer, where $\overline{u}_x$ is the average displacement in the competent layer and v_x is the displacement that would occur in the matrix if the competent layer were absent. This term has the form of the shear-lag model first introduced by Cox (1952) and is used as the foundation of many previous models of joint spacing (e.g. Ji and Saruwatari, 1998; Hu and Evans, 1989). The essential feature in using the shear-lag model rests in establishing an approximation for the spring constant k that matches the two-dimensional behavior of the strained matrix–competent layer system. In the version of the shear-lag model proposed by Ji and Saruwatari (1998), an approximate form for the decay of the shear stress in the matrix layer (in the direction normal to the interface) is assumed, resulting in the spring constant

$$k = \frac{bE_m}{2M(1+\nu_m)}, \tag{12}$$

where ν_m is the Poisson's ratio of the matrix;

$$M = \int_{t/2}^{(t+d)/2} \left(\frac{d+t-2y}{d-t+2y}\right)^n dy, \tag{13}$$

and n is an integer. With the value of $n = 3$ as suggested by Ji and Saruwatari (1998), the integral in Eq. (11) can be evaluated to give $M = (3\log 2 - 2)d$ where d is the thickness of the matrix layer.

The second component on the right-hand-side of Eq. (10) accounts for the slip region where τ_f is the shear stress at failure. Within the framework of the Mohr–Coulomb failure criterion adopted in this study,

$$\tau_f = c + \gamma h \tan\phi, \tag{14}$$

where c is the cohesion and ϕ is the friction angle characterizing the matrix–competent layer interface (e.g. Goodman, 1989).

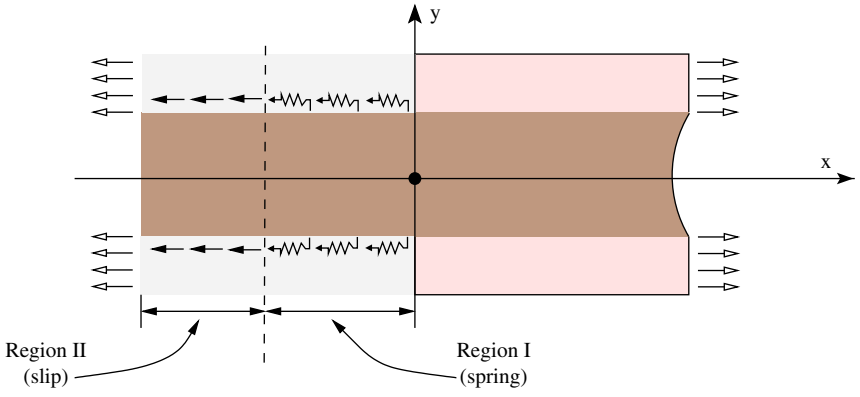

Fig. 4. Mechanical analog of the competent layer–matrix system.

By definition, the average extensional strain in the matrix is

$$\epsilon = \frac{\mathrm{d}v_x}{\mathrm{d}x}; \tag{15}$$

the shear stress at failure in Eq. (14) is independent of x, and the axial stress in the competent layer can be written by virtue of Eq. (2) as

$$\sigma_x = E_c \frac{\mathrm{d}\overline{u}_x}{\mathrm{d}x}. \tag{16}$$

Hence, Eq. (11) can be differentiated with respect to x to give

$$\frac{\mathrm{d}^2\sigma_x}{\mathrm{d}x^2} = -\begin{cases} \dfrac{2k(\epsilon - \sigma_x/E_c)}{A}, & 0 \le x \le x_t \\ 0, & x_t \le x \le \dfrac{\lambda}{2} \end{cases}, \tag{17}$$

subject to boundary conditions

$$\frac{\mathrm{d}\sigma_x}{\mathrm{d}x}(0) = 0, \quad \sigma_x\left(\frac{\lambda}{2}\right) = 0, \tag{18}$$

where the first equation in Eq. (18) is driven by the symmetry of the problem. Beyond Eq. (18), the stress component σ_x must also satisfy the continuity conditions at the transition ($x = x_t$) from the slip to no-slip region, namely

$$\sigma_x\left(x_t^-\right) = \sigma_x\left(x_t^+\right) = \frac{2\tau_f}{t}\left(\frac{\lambda}{2} - x_t\right). \tag{19}$$

The solution that satisfies Eqs. (17)–(19) can be obtained as

$$\sigma_x = -\begin{cases} E_c\epsilon\left\{1 - \dfrac{\cosh(\beta x)}{\cosh(\beta x_t)}\left(1 - \beta\eta\left(\dfrac{\lambda}{2} - x_t\right)\right)\right\}, & 0 \le x \le x_t \\ \dfrac{2\tau_f}{t}\left(\dfrac{\lambda}{2} - x\right), & x_t \le x \le \dfrac{\lambda}{2} \end{cases}, \tag{20}$$

where

$$\beta = \sqrt{\frac{2k}{E_c A}}, \quad \eta = \frac{\beta\tau_f b}{k\epsilon}, \tag{21}$$

and k is calculated from Eq. (12) with $M = (3\log 2 - 2)d$.

In Eq. (20), the location of x_t of the transition from no-slip to slip region is unknown. Two steps are required to find this location. In the first place the value of η in Eq. (21) is used to determine if, for a given applied strain ϵ and intact segment length λ, slip can occur in the system. It can be shown that the value of the slope of the stress, calculated from the first component of Eq. (20), will always be less than $2\tau_f/t$, thereby precluding slip whenever $\eta \ge 1$ (see Timm et al., 2003). If, on the other hand, the value of η is <1 and the length of the competent layer $\lambda \ge (2/\beta)\tanh^{-1}(\eta)$, a part of the interface between the competent layer and the matrix will slip. Under this condition, the value of the transition point x_t can be found from Eq. (6) which requires that

$$\frac{\mathrm{d}\sigma_x}{\mathrm{d}x}\left(x_t^-\right) = \frac{\mathrm{d}\sigma_x}{\mathrm{d}x}\left(x_t^+\right) = -\frac{2\tau_f}{t}. \tag{22}$$

On the basis of Eqs. (20) and (22), one arrives at the nonlinear equation

$$x_t = \frac{1}{\beta}\tanh^{-1}\left(\frac{\eta}{1 - \beta\eta\left(\dfrac{\lambda}{2} - x_t\right)}\right), \quad 0 < x_t < \lambda/2; \tag{23}$$

for x_t which can be rearranged as

$$x_t = \frac{\lambda}{2} + \frac{1}{\beta\eta}\left(\frac{\eta}{\tanh(\beta x_t)} - 1\right); \tag{24}$$

a more stable basis for an iterative solution in terms of x_t.

4. Applicability of the 1D analysis

In Timm et al. (2003), it was shown that the one-dimensional (1D) stress distribution model provides a good approximation of the so-called "thin film" 2D systems wherein the thickness of the fractured layer is at least an order of magnitude smaller than all other characteristic lengths of the problem. For the situation at hand, however, the latter assumption often does not hold and it is necessary to investigate the applicability of formula (20) to layered rock beds where the competent layer thickness (t) may be comparable to its matrix counterpart (d), joint spacing (λ), or both. To this end, it is instructive to adopt the problem parameters as in Bai and Pollard (2000b) who assumed $E_c = E_m = 30$ GPa, $\nu_c = \nu_m = 0$, 25, $t = 0.2$ m, and $d = 0.6$ m. This configuration is also similar to that in Bai and Pollard (2000a) who assumed $E_c = E_m = 40$ GPa and demonstrated, via numerical simulations, that the ratio E_c/E_m has only a limited effect on the stress distribution between the joints.

In what follows, the 2D stress analysis of the competent layer is performed using the finite element code FEMLAB 3 (www.femlab.com) for two characteristic cases, namely (i) the no-slip regime ($x_t = \lambda/2$) as in Bai and Pollard (2000a,b), and (ii) the full-slip case ($x_t = 0$). For these two configurations, the representative domain and the relevant boundary conditions are assumed as in Fig. 5 by making use of the problem symmetries in Eq. (1). To ensure the accuracy of the plane stress analysis, all finite element calculations are performed with an adaptive mesh consisting of no less than 17,000 quadratic triangular (Lagrange) elements.

With reference to the definitions in Eq. (2), the left panel in Fig. 6 compares the *average* axial stress in the competent layer

$$\sigma_x(x) = \frac{1}{t}\int_{-t/2}^{t/2} \sigma_{xx}(x,y)\mathrm{d}y,$$

stemming from the 2D finite element analysis, with its one-dimensional approximation (20) assuming joint-spacing-to-layer-thickness ratios $\lambda/t = 1$, 2, 5 and 10. As can be seen

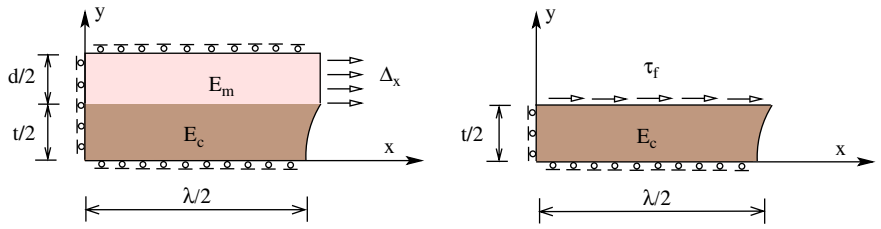

Fig. 5. Two-dimensional stress analysis: representative domain and boundary conditions for the no-slip case (left) and the full-slip case (right).

from the display the 1D model, despite its simplicity, maintains a reasonable approximation of the more complex 2D case, even for the "short" joint spacing $\lambda/t = 1$. One may further note that, consistent with Bai and Pollard (2000a,b), the finite element analysis used to generate the "no-slip" data indeed indicates the presence of a compressive axial stress (σ_{xx}) in the middle of the competent layer for ratios $\lambda/t < 0.97$ when $E_c = E_m$.

For completeness, the right panel in Fig. 6 plots the average axial stress, σ_x, computed using finite element simulations for the full-slip situation $x_t = 0$. In this case, the variation of σ_x is indistinguishable from the linear 1D pattern given by the second equation in Eq. (20), see also Fig. 3. With reference to the full-slip configuration in Fig. 5, this result should not be surprising as it simply confirms that the finite element solution satisfies the static equilibrium on each of its segments $[x, \lambda/2]$. Indeed, this equilibrium argument must hold for *any* joint-spacing-to-layer-thickness ratio, and thus the observed linear variation of σ_x applies equally for the range $0 < \lambda/t < 1$. In other words, under a full-slip condition, the shear-lag model is valid for *all* joint-spacing-to-layer-thickness ratios.

5. Characteristic joint spacing

By virtue of Eq. (20), the maximum stress in a competent layer of intact length λ is given by

$$\sigma_{x,\max} = \sigma_x(0) = E_c\epsilon\left\{1 - \frac{1}{\cosh(\beta x_t)}\left(1 - \beta\eta\left(\frac{\lambda}{2} - x_t\right)\right)\right\}. \tag{25}$$

On equating this stress to the apparent (prestress-augmented) tensile strength S' according to Eq. (10), an equation for the characteristic joint spacing $\lambda = \lambda_c$ is obtained in the form

$$\lambda_c(\epsilon, h) = 2x_t + \frac{2}{\beta\eta}\left(1 + \left[\frac{S' - E_c\epsilon}{E_c\epsilon}\right]\cosh(\beta x_t)\right). \tag{26}$$

Eq. (26) is non-linear since by Eqs. (23) or (24) the extent of the no-slip region, x_t, depends on λ_c. Accordingly, obtaining the characteristic joint spacing from Eq. (25) requires the following steps:

1. Check whether $E_c\epsilon > S'$; if this condition is not satisfied, stresses in the competent layer cannot reach a level where fracture can occur and thus $\lambda_c \to \infty$.
2. Calculate the values of M, k, β, and η from Eqs. (12), (13), and (21).
3. If $\eta \geq 1$, set $x_t = \lambda_c/2$ and jump to Step 5.
4. With the current estimate of λ_c, check whether $\lambda_c \geq (2/\beta)\tanh^{-1}(\eta)$. If so, solve (24) for x_t iteratively using $\lambda = \lambda_c$; otherwise set $x_t = \lambda_c/2$.
5. Evaluate λ_c from Eq. (26) using the current estimate of x_t.
6. If the pre-defined convergence tolerance in terms of λ_c is not met, go to Step 3.

5.1. Limit cases and saturation spacing

Before the behavior of the joint spacing model Eq. (26) is investigated in more detail, it is worthwhile to establish some limit cases.

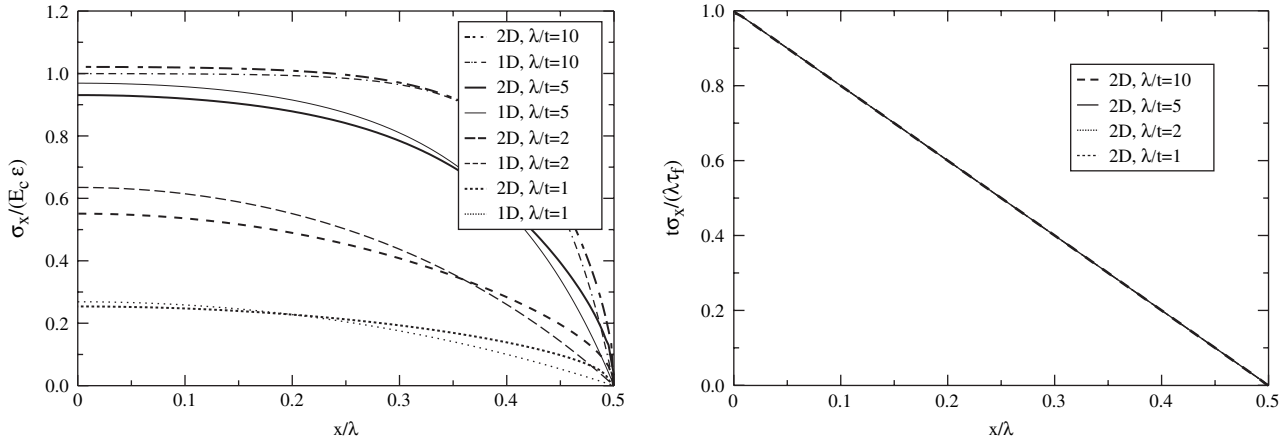

Fig. 6. Average axial stress distribution, σ_x, in the competent layer for the no-slip case (left) and the full-slip case (right).

5.1.1. The no-slip case

First consider the case on a given applied strain ϵ. At a sufficiently large depth h, conditions $\eta < 1$ and $\lambda_c \geq (2/\beta)\tanh^{-1}(\eta)$ will not hold and the matrix and competent layers will be perfectly bonded, i.e. $x_t = \lambda/2$. Under this condition, Eq. (26) reduces, as required, to the explicit joint spacing model proposed by Ji and Saruwatari (1998) where

$$\lambda_c(\epsilon, h) = \frac{2}{\beta}\cosh^{-1}\left[\frac{E_c\epsilon - S'}{E_c\epsilon}\right], \quad h \to \infty. \tag{27}$$

One may note that the no-slip limit in Eq. (27) can alternatively be obtained by letting the cohesion $c \to \infty$ in Eq. (14).

5.1.2. The full-slip case

On the other hand, as the applied strain ϵ is increased, the no-slip region at a given depth will diminish i.e. $x_t \to 0$, see curve "d" in Fig. 2. As a result, $\cosh(\beta x_t) \to 1$ so that, by virtue Eqs. (21) and (26), one arrives at the lower bound on joint spacing

$$\lambda_c(\epsilon, h) = \lambda_c^{\min} \equiv \frac{S't}{\tau_f}, \quad \epsilon \to \infty; \tag{28}$$

that defines *fracture saturation* (e.g. Bai and Pollard, 2000a,b; Bai et al., 2000). Two comments are in order at this point. First, an essentially identical saturation limit has been developed for engineered systems, e.g. strained thin ceramic films (see discussion in Timm et al., 2003) where such limiting values for the joint (i.e. crack) spacing are experimentally observed (Chen et al., 1999). Secondly, on setting $S' = S$, the rigorously derived limit in Eq. (28) yields the saturation spacing that is twice the value obtained in Ji et al. (1998). With reference to Fig. 1, this disagreement stems from the fact that the present analysis incorporates the interfacial shear stress at failure, τ_f, from *both* the upper ($y = t/2$) and lower ($y = -t/2$) layer–matrix interfaces; a feature apparently overlooked in the earlier study.

In relating to a geology context, three features of the expression (28) for fracture saturation are highlighted. First, one may note the limiting value of joint spacing varies *linearly* with the competent layer thickness t; a feature that is repeatedly observed in the field (e.g. Narr and Suppe, 1991; Gross, 1993; Ji and Saruwatari, 1998). Secondly, due to extended validity of the shear-lag model under the condition of full slip at the layer–matrix interface (see Section 4), the saturation limit Eq. (28) is valid for *all* joint-spacing-to-layer-thickness ratios. This is an important result as it offers a mechanism for the saturation limit on joint spacing that is not only alternative to that proposed in Bai and Pollard (2000a,b), but also provides a rational explanation of the "closely-spaced" joints, observed in nature at λ/t ratios significantly less than unity (e.g. Ladeira and Price, 1981); a situation that is not permitted by the earlier model. Finally, by virtue of Eqs. (9), (10) and (14), expression (28) for fracture saturation can be rewritten as

$$\frac{\overline{\lambda}_c(\epsilon, h)}{t} = 0.75\,\frac{S + \gamma h \nu_c}{c + \gamma h \tan\phi}, \quad \epsilon \to \infty. \tag{29}$$

This form of the limiting expression clearly illustrates the opposing effects of the overburden depth h on joint spacing as it simultaneously i) increases the spacing via the Poisson effect in the numerator, and ii) decreases its value via the Mohr–Coulomb failure criterion in the denominator.

6. Results

A main focus of this paper is to understand the effects of overburden depth on the average joint spacing (9) in stratified rock systems. In the aforementioned analysis, these effects are observed both in the definition of the *apparent* tensile strength of the competent layer (10) and the interfacial shear strength according to Eq. (14). In what follows, these influences are examined in Fig. 7 using the elastic and geometric parameters as in Ji and Saruwatari (1998). The Figure shows three sets of results, where "slip & prestress" denotes the full solution; "slip only" is the special case where the prestress term $\nu_c\gamma h$ in Eq. (10) is neglected; and "prestress only" is the solution obtained by artificially setting $\phi = 0$ and assigning an arbitrary high value to the cohesion c. In the diagram, a field-observed joint spacing reported in Ji and Saruwatari (1998) corresponding to the featured set of elastic parameters is also indicated by the horizontal dashed line; this value is only provided as a point of reference and it does not convey the spread that is intrinsically present in the complete field data.

As shown in Fig. 2, the interfacial shear stress between the competent layer and the matrix at a given depth varies monotonically along the length of the intact segment. It has maximum *absolute* values at the ends of the segment, and a value of zero at the center. Therefore, a slip will propagate from the ends of the segment inward with increasing tectonic strain (see also Ji et al., 1998 and Timm et al., 2003). As the overburden depth increases, however, the interfacial shear *strength*

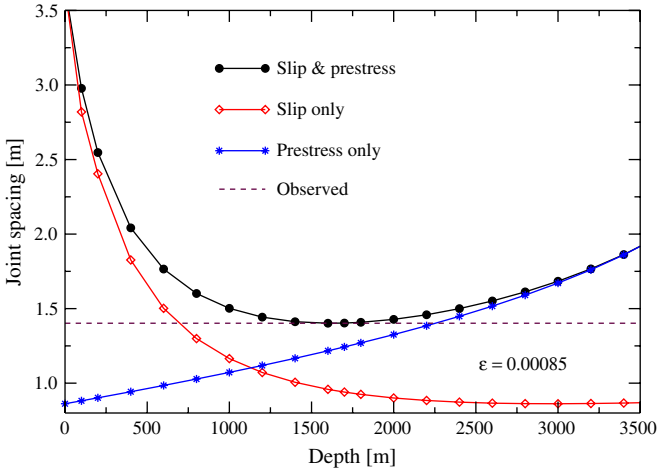

Fig. 7. Average joint spacing ($0.75\lambda_c$) calculated using the slip & prestress, slip only, and prestress only solutions. Model parameters: $t = 1.2$ m, $d = 0.62$ m, $E_c = 58$ GPa, $E_m = 16$ GPa, $\nu_c = \nu_m = 0.25$, $\gamma = \rho g = 24$ kN/m^3, $S = 20$ MPa, $c = 5$ MPa, and $\phi = 30°$.

increases according to Eq. (14), the length of the slip region $\lambda - x_t$ decreases and, for a given tectonic strain, the tensile stress in the competent layer builds up (see Fig. 3). In this way, the joint spacing decreases with depth as shown by the curve labeled "slip only" in Fig. 7.

In contrast, if slip does not occur (e.g. the cohesion c is sufficiently high), the overburden depth enters the solution exclusively through the prestress term $\nu_c \gamma h$ in Eq. (10) that increases the apparent strength of the competent layer. In this way, the joint spacing increases with depth as shown by curve "prestress only" in Fig. 7.

The full, "slip & prestress" solution incorporating the effects of overburden via both slip and compressive prestress, shows the combined effect of the above trends versus depth. The initial decrease in joint spacing indicates that the overburden pressure-induced reduction of slip dominates the response up to a depth of approximately one kilometer. Beyond this value, the interfacial slip becomes negligible and the increase in the apparent shear strength according to Eq. (14) takes a lead role in controlling the joint spacing.

The results in Fig. 7 are all generated assuming $\epsilon = 0.00085$ for the applied tectonic strain. This value was chosen so that the minimum "Slip & prestress" joint spacing matches the reference field observations. For completeness it is noted that the calculated value of the tectonic strain, reported by Ji & Saruwatari, 1998 on the basis of the "no prestress – no-slip" solution is $\epsilon^{JS} = 0.0005$. In this context, it is worthwhile to examine the effect that the layer depth (at the time of joint formation) has on the value of the *estimated* tectonic strain. This is illustrated in Fig. 8 which plots joint spacings with depth for different values of applied strain. As can be seen from the graph, for a given observed value of joint spacing, estimated-tectonic-strain solution in terms of ϵ may have multiple solutions depending on the assumption of the "original" depth of the competent layer. In particular, one may note that, whereas a strain value of 0.0004 fails to reach the reference joint spacing, a strain value of 0.0016 will match the reference joint spacing at two different depths.

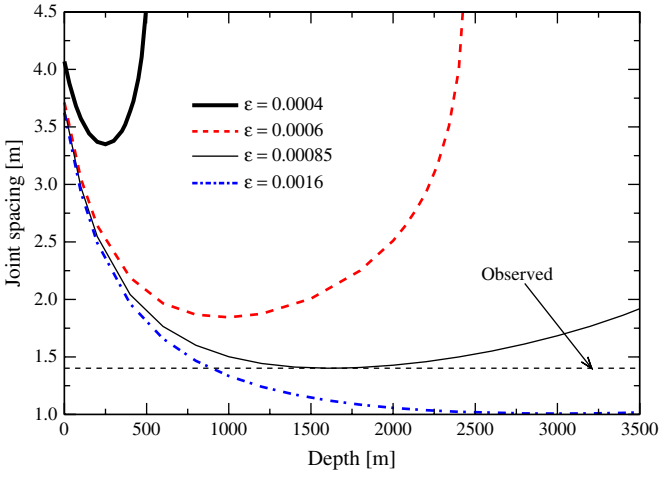

Fig. 8. Average joint spacing ($0.75\lambda_c$) calculated using the full (slip & prestress) solution under varying levels of applied tectonic strain ϵ. Model parameters: $t = 1.2$ m, $d = 0.62$ m, $E_c = 58$ GPa, $E_m = 16$ GPa, $\nu_c = \nu_m = 0.25$, $\gamma = 24$ kN/m^3, $S = 20$ MPa, $c = 5$ MPa, and $\phi = 30°$.

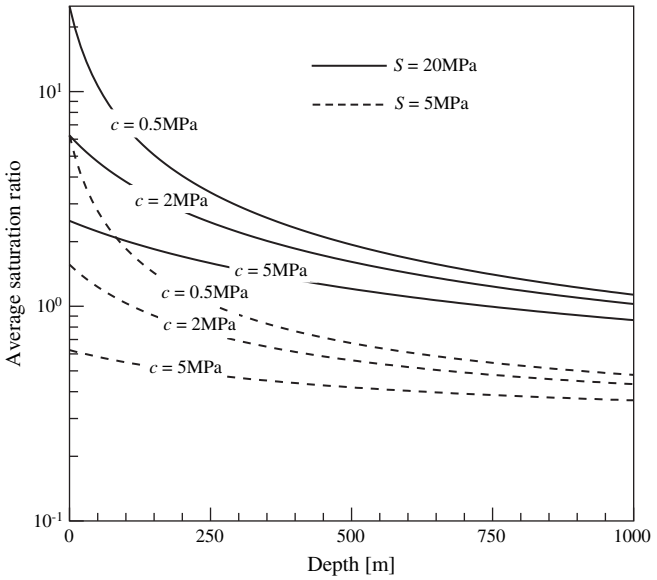

Fig. 9. Average joint-spacing-to-layer-thickness ratio at saturation, $\lim_{\epsilon\to\infty}(\overline{\lambda}_c/t)$, versus overburden depth. The remaining material parameters are the same as in Fig. 8.

Another goal of this work is to quantify the relationship between the joint spacing and the competent layer thickness, in particular for the case when joint saturation is reached. To this end, the behavior of Eq. (29) under various conditions is investigated; recall that, due to its derivation under a full interface slip condition, this expression is valid for all joint-spacing-to-layer-thickness ratios. As an illustration, Fig. 9 plots the ratio between the (average) saturation joint spacing and the competent layer thickness, $\lim_{\epsilon\to\infty}(\overline{\lambda}_c/t)$, against overburden depth h for various values of the interfacial cohesion c and tensile strength S of the competent layer. The predicted values span the range of field observations; Bai and Pollard (2000b), for example, cite ratios in the range 0.1–10. Of particular note are the field-consistent predictions of saturation-spacing-to-thickness ratios below unity. This is contrast to the previous works (Bai and Pollard, 2000a,b) where the no-slip, 2D analysis of layered systems indicates that no sufficient tensile stresses can be generated in competent layer (under any strain) to induce cracking for the ratios $\overline{\lambda}_c/t < 1$. Hence, limit (29) demonstrates that the interfacial slip, manifest via the strength parameters c and ϕ, provides a plausible and valid explanation for the field-observed saturation ratios $\overline{\lambda}_c/t < 1$.

7. Conclusions

A principal objective of a model of joint spacing in sedimentary rocks is to be able to estimate, via matching model joint spacing predictions to field observations, the tectonic strain during the formation of geological structures. Previous work has shown that the mechanics that relates the joint spacing observed in layered sedimentary rock systems to the applied tectonic strain can be explained by an application of

shear-lag models. A shortcoming of the reported shear-lag models is that they do not explicitly account for the effect of overburden depth. With increasing depth of overburden, on the one hand, the shear strength of the interface between the competent layer and the matrix increases; as a result, the amount (length) of slip along the interface decreases. For a given strain, a decrease in slip in turn leads to an increase in the stress transferred to the competent layer and a reduction in the observed joint spacing. On the other hand, an increase in overburden depth also increases the horizontal prestress and consequently the apparent tensile strength of the competent layer, resulting in a longer joint spacing. This paper has shown that when overburden depth is included in the shear-lag model, due to the interplay between the opposing effects of shear strength and prestress, the predictions of joint spacing with depth take a characteristic convex-down shape with the minimum value observed at an intermediate depth. This suggests that an estimate of the tectonic strain undergone by the earth's crust might require knowledge of both the joint spacing and the depth of the layer when the joints were formed. This hypothesis, based on a rigorous development of the mechanics, needs to be confirmed by the field observations.

Another aspect of the present study is to re-establish the applicability of the shear-lag model as a reasonable ''first-cut'' analysis tool for structural geology. In particular, this 1D model is shown to be (i) consistent with the 2D equilibrium equations in an average (integral) sense, (ii) physically applicable for joint-spacing-to-thickness ratios down to unity, and (iii) *universally* applicable under the condition of full slip between the competent layer and its matrix. This last feature results in an explicit formula for the variation of the saturation joint spacing with depth; a result that leads to, within the choice of realistic physical parameters and overburden depths, predicted values of the joint-spacing-to-thickness ratio that span the range of values observed in the field. In particular, this result provides a theoretically valid explanation for the field-observed joint spacings with a joint-spacing-to-thickness ratio below unity.

In conclusion, it is noted that although the proposed engineering model does provide a sound theoretical argument for the features and trends of field-observed joint spacings, it nonetheless operates in a ''clean'' environment. In reality, the natural variations within the rock strata will inevitably influence the observed joint spacing. For example, inherent flaws in the competent layer will reduce the apparent tensile strength, decrease the joint spacing, and increase the calculated spread in the field observations for a given layered system.

Acknowledgment

This work is partially supported by the National Center for Earth-surface Dynamics (NCED), a Science and Technology Center funded by the Office of Integrative Activities of the National Science Foundation. The authors would also like to thank the journal reviewers and editors, their comments have made a significant contribution to the quality of this paper.

References

Bai, T., Pollard, D.D., 2000a. Fracture spacing in layer rocks: a new explanation. Journal of Structural Geology 22, 43–57.

Bai, T., Pollard, D.D., 2000b. Closely spaced fractures in layered rocks: initiation mechanism and propagation kinematics. Journal of Structural Geology 22, 1409–1425.

Bai, T., Pollard, D.D., Gao, H., 2000. Explanation for fracture spacing in layered materials. Nature 403, 753–755.

Chen, B.F., Hwang, J.F., Yu, G.P., Huang, J.H., 1999. In situ observation of the cracking behavior of TiN coating on 304 stainless steel subjected to tensile strain. Thin Solid Films 352, 173–178.

Cox, H.L., 1952. The elasticity and strength of paper and other fibrous materials. British Journal of Applied Physics 3, 72–79.

Goodman, R.E., 1989. Rock Mechanics, second ed. John Wiley & Sons, New York.

Gross, M.R., 1993. The origin and spacing of cross joints: examples from the Monterey Formation, Santa Barbara Coastline, California. Journal of Structural Geology 15, 737–751.

Guzina, B.B., Voller, V.R., Timm, D.H., 2004. Crack spacing in strained films. Journal de Physique IV 124, 201–208.

Hobbs, D.W., 1967. The formation of tension joints in sedimentary rocks: an explanation. Geology Magazine 104, 550–556.

Hu, M.S., Evans, A.G., 1989. The cracking and decohesion of thin films on ductile substrate. Acta Metallurgica et Materialia 37, 917–925.

Ji, S., Saruwatari, K., 1998. A revised model for the relationship between joint spacing and layer thickness. Journal of Structural Geology 20, 1495–1508.

Ji, S., Zhu, Z., Wang, Z., 1998. Relationship between joint spacing and bed thickness in sedimentary rocks: effects of interbed slip. Geology Magazine 135, 637–655.

Ladeira, F.L., Price, N.J., 1981. Relationship between fracture spacing and bed thickness. Journal of Structural Geology 3, 179–183.

Malvern, L.E., 1969. Introduction to the Mechanics of a Continuous Medium. Prentice-Hall, New Jersey.

Mandal, N., Deb, S.K., Khan, D., 1994. Evidence for a non-linear relationship between fracture spacing and layer thickness. Journal of Structural Geology 16, 1275–1281.

Narr, W., Suppe, J., 1991. Joint spacing in sedimentary rocks. Journal of Structural Geology 13, 1037–1048.

Timm, D.H., Guzina, B.B., Voller, V.R., 2003. Prediction of thermal cracking. International Journal of Solids and Structures 40, 125–142.

Zhao, P., Ji, S., 1997. Refinements of shear-lag model and its applications. Tectonophysics 279, 37–53.